THE ASTROPHYSICAL JOURNAL, 192:293–310, 1974 September 1

PHOTOMETRIC PROPERTIES OF MODEL SPHERICAL GALAXIES

RICHARD B. LARSON
Yale University Observatory
AND
BEATRICE M. TINSLEY
The University of Texas at Dallas; and Astronomy Department, The University of Texas at Austin
Received 1974 February 25

ABSTRACT

This paper presents the results of detailed calculations of the photometric properties of the dynamical models for the formation and evolution of spherical galaxies recently computed by Larson. The models that were found in Paper I to have radial density distributions closely matching those of elliptical galaxies are found to resemble elliptical galaxies also in their colors, mass-to-luminosity ratios, and narrow-band spectral energy distributions. However, the residual star formation activity in the nuclei of these models makes the nuclear colors bluer than normal, suggesting that most elliptical galaxies have lost their residual gas and do not experience current star formation. The effect of the metal abundance gradient of Paper I on the colors has been estimated, and (in the absence of current star formation) it causes the nucleus of a galaxy to appear redder than the outer regions, as is generally observed. The models with expanding boundaries, in which star formation continues to be important at the present time, have colors and mass-to-luminosity ratios which resemble those of spiral galaxies, showing that differences in the photometric properties of different types of galaxies can be understood in terms of different dynamical histories. The evolution of the photometric properties of the models is discussed, and it is concluded that continuing star formation in elliptical galaxies is not likely to affect significantly the rate at which they evolve in color and luminosity. The predicted supernova rates in models whose *UBV* colors resemble those of different Hubble types of galaxies agree with the observed supernova rates in these types of galaxies.

Subject headings: galactic structure — galaxies, photometry of — star formation — supernovae

I. INTRODUCTION

In a previous paper Larson (1974, hereafter Paper I), results were presented for a number of dynamical models describing the formation and evolution of spherical galaxies. It was shown in that paper that when plausible assumptions are adopted for the initial conditions and the star formation and gaseous dissipation rates, it is possible to obtain models whose radial density distributions agree closely with those of elliptical galaxies; furthermore, when a conventional stellar mass spectrum is assumed and the production of heavy elements is calculated, metal abundance distributions are obtained which also resemble the observations. In the present paper we describe the results of detailed calculations of the photometric properties of these models (i.e., their colors, luminosities, and related properties), and we compare these predicted photometric properties with observations of various types of galaxies. In particular, we wish to compare with observations of elliptical galaxies the properties of those models which were found in Paper I to have density distributions closely matching those observed for elliptical galaxies. This comparison provides an important constraint on the models and should be useful for improving our understanding not only of the present stellar content of elliptical galaxies but also of their past evolution, and hence for interpreting the properties of galaxies observed at cosmological distances.

We also discuss some properties of the "expanding boundary" models of Paper I; because of the prolonged time scale for collapse of the outer layers of the initial protocloud in these models, star formation is still going on at a significant rate after 12×10^9 years. Although these spherical models cannot be expected to resemble flattened rotating systems in any detail, it is of interest to see whether their photometric properties resemble those of later-type (spiral) galaxies which appear to have similar rates of star formation.

The calculations of Paper I yield directly the star formation rate as a function of time and radial coordinate r throughout the evolution of the system. In order to calculate the present photometric properties of the model, it is necessary to know the complete past history of star formation for those stars presently located in each radial zone; this has been obtained as described in Paper I by using mean stellar velocities to follow the radial motion of the stars as the system evolves. Since the structure of an elliptical galaxy does not change significantly after the first few billion years, the resulting present radial distributions of stellar populations can be used also to calculate the photometric properties of galaxies at most observable distances. Once the complete history of star formation is known for each radial zone, the distribution of stars in the Hertzsprung-Russell diagram can be determined as a function of time and the photometric properties of each zone can be calculated using the methods described by Tinsley (1972*a*).

The data on stellar evolution, bolometric corrections, colors, and spectral energy distributions used in this

investigation have been described by Tinsley (1972*a*). The late stages of evolution of stars near 1 $M_\odot$ are particularly important in determining the photometric properties of systems of predominantly old stars, and the effects of uncertainties in these stages of evolution have been studied by Rose and Tinsley (1974). For red giants near 1 $M_\odot$ we have used the "case B" evolutionary tracks discussed in these two papers. The theoretical and semiempirical evolutionary tracks and photometric calibrations used are appropriate for stars with the chemical composition of the old galactic disk population, i.e., approximately the solar composition.

The models of Paper I all develop a metal abundance gradient in (at least) the nuclear region, where the metal abundance increases strongly toward the center. This result is in qualitative agreement with many observations indicating the presence of composition gradients in the stars and gas of elliptical and spiral galaxies (McClure 1969; Spinrad *et al.* 1971; Spinrad, Smith, and Taylor 1972; Welch and Forrester 1972; Janes 1972; Searle 1971). Since the metal abundance has an important effect on the evolution and photometric properties of stars, the composition gradient must be taken into account in a proper calculation of the photometric properties of a galaxy as a function of radial position. Unfortunately, our knowledge of the effects of metal abundance on the evolution and photometric properties of stars is not sufficient to allow detailed calculations to be made for nonsolar metal abundances. Instead, we have adopted an approximate procedure whereby all properties are first calculated assuming solar metal abundances for all stars, and then differential corrections are estimated for nonsolar abundances. (Only the $B - V$ color has been corrected in this way, since there is insufficient information to allow other photometric properties to be corrected in the same way.)

In § II we summarize from Paper I the characteristics of each model which mainly determine its photometric properties. In § III we give results for the present photometric properties of the models and compare them with the observations, and in § IV we discuss the evolution of the colors and magnitudes and compare the results with data for distant elliptical galaxies. The principal conclusions are summarized in § VI, and the Appendix gives a description of the method used to correct the $B - V$ colors for nonsolar metal abundances.

II. MODEL CHARACTERISTICS AND STAR FORMATION RATES

The dynamical models of Paper I were calculated with various assumptions concerning the initial and boundary conditions, the star formation and gaseous dissipation rates, and the initial stellar mass function (IMF). The photometric properties of any zone of a model are determined by the time dependence of the star formation rate and by the initial stellar mass function, which is assumed to be independent of time and position. We consider first the properties of models A–D and F of Paper I, which were found to have radial density distributions closely resembling those of elliptical galaxies; we also give some results for the "expanding models" H and I, which have high present rates of star formation. The model characteristics that are relevant to the determination of their photometric properties are briefly summarized below. In all cases the total mass is $10^{11}\ M_\odot$.

Model A has a fixed boundary radius of 30 kpc, and the star formation and gaseous dissipation time scales are assumed to be approximately equal to the dynamical time scale. The initial mass function (IMF) is logarithmically Gaussian, as suggested by the probabilistic fragmentation theory of Larson (1973), and it approximates the IMF of the solar neighborhood, except for the recently discovered excess of late M dwarfs (e.g., Weistrop 1972). To allow for the extra mass in these faint dwarfs and to obtain an average metal abundance which is approximately solar, only half of the mass has been assigned to the Gaussian mass spectrum, and the remainder to additional low-mass "invisible objects." This procedure is justified by the fact that Rose and Tinsley (1974) studied the photometric properties of a model with the IMF of the solar neighborhood and found that the late M dwarfs contribute negligibly to the light of the system, which is dominated by giants.

Model B has the same dynamical characteristics as model A, but the IMF is the well-known Salpeter law:

$$dN/dm \propto m^{-(1+x)} \qquad (1)$$

with

$$x = 1.35\,, \qquad 0.02 < m/m_\odot < 50\,.$$

The resulting average metal abundance depends in this case on the lower mass limit, and is approximately solar for a lower limit of 0.02 $m_\odot$. The power law (1) is not a very accurate representation of the solar neighborhood IMF; although it fits the more massive stars fairly well, the stars below 1 $M_\odot$, which are more important for elliptical galaxies, have a shallower IMF corresponding to $x \sim 0.5$.

Model C differs from model B only in that the lower mass limit in equation (1) is 0.04 $m_\odot$ instead of 0.02 $m_\odot$; this results in a higher metal abundance and a lower mass-to-luminosity ratio than for model B.

The IMFs of models A, B, and C are illustrated in figure 1 of Paper I. These three models are dynamically almost identical, and they have density distributions that closely match the observed intensity profile of NGC 3379 (Miller and Prendergast 1962), as shown in figure 3 of Paper I. The models described below all have the same IMF as model B.

Model D has a boundary radius of 50 kpc instead of 30 kpc, and this results in a somewhat longer time scale for collapse and star formation. Also, as discussed in Paper I, the more extended density profile of model D may provide a slightly better fit to most elliptical galaxies than models A–C. In its photometric properties, model D is nearly identical to model B.

Model F differs from model D in that the star formation rate is assumed to depend only on a power of the local gas density (in this case, the 1.85 power); likewise, the gaseous dissipation rate depends only on

the local gas density and velocity dispersion. As a result, during the later stages of evolution, the residual gas and star formation activity become much more strongly concentrated toward the center than in models A–D.

Model H has an expanding boundary, and this greatly lengthens the time required for the outer regions of the initial protocloud to fall into the forming galaxy and become transformed into stars; therefore, star formation continues throughout the system at a significant rate up to the present epoch.

Model I is like model H except that the star formation and gaseous dissipation rates depend on the local gas properties, as in model F. Star formation thus continues at a significant rate up to the present time as in model H, but becomes increasingly concentrated in the nucleus, as in model F.

The integrated photometric properties of the models depend mainly on the total star formation rate as a function of time; this quantity is illustrated in figure 1 for the models described above. For models A–D and F, whose radial structure closely resembles that of elliptical galaxies, nearly all of the star formation takes place during the first $\sim 2 \times 10^9$ years, and subsequent star formation has a relatively unimportant effect on most of the properties of interest. Thus the integrated photometric properties should not differ greatly from those of the "single burst" models of Tinsley (1972*c*) in which star formation is limited to the first 10^9 years; these models were found to have spectral energy distributions very similar to those of elliptical galaxies. Models H and I will, of course, show much more important contributions from young stars in their integrated light, and they should therefore look (photometrically) more like spiral galaxies.

The relative importance of young stars for the photometric properties of the different zones of a model depends on the relative present stellar birthrate; this is shown as a function of radius in figure 2, at an assumed present age of 11×10^9 years for all models. In all models, the greatest present rate of star formation occurs in the nuclear region, owing to the continuing infall of residual gas into the nucleus. Thus the nucleus always contains the highest proportion of young stars, and in the absence of other effects it would appear bluer than the rest of the galaxy (see § III).

Star formation continues up to the present time in all models, albeit at a rapidly decreasing rate, since we have assumed that any gas present or produced in a galaxy always remains in the galaxy and forms new stars. It is possible, however, that in reality continuing star formation does not occur in most elliptical galaxies, since a "galactic wind" produced by supernova heating of the gas may sweep out the residual gas from a galaxy during the later phases of its evolution (Mathews and Baker 1971; see also Yahil and Ostriker 1973). A rough estimate of the supernova heating effect in the present model shows that this effect may become large enough to produce a galactic wind as early as $1–2 \times 10^9$ years after the formation of the galaxy, although there is a large uncertainty in this estimate. To investigate the effect which such gas loss might have on the photometric properties of a galaxy, we have made some test calculations with model B in which star formation is arbitrarily cut off at various times. We find that within 10^9 years after star formation ceases, the colors become almost identical to those of a "single burst" model in which star formation is cut off after the first 10^9 years; in other words, the photometric properties are almost entirely determined by the stars formed during the first 10^9 years and by the youngest stars formed within the past 10^9 years. Thus we can illustrate the possible effect of gas loss on the photometric properties of a galaxy by presenting some results for a "single burst" model:

Model S is a single burst model with the same IMF as model B but with star formation arbitrarily cut off

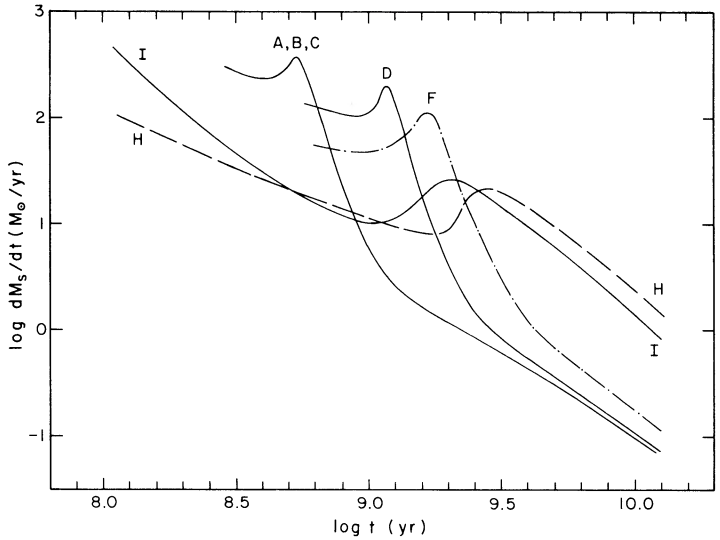

FIG. 1.—The total star formation rate versus time for the models studied

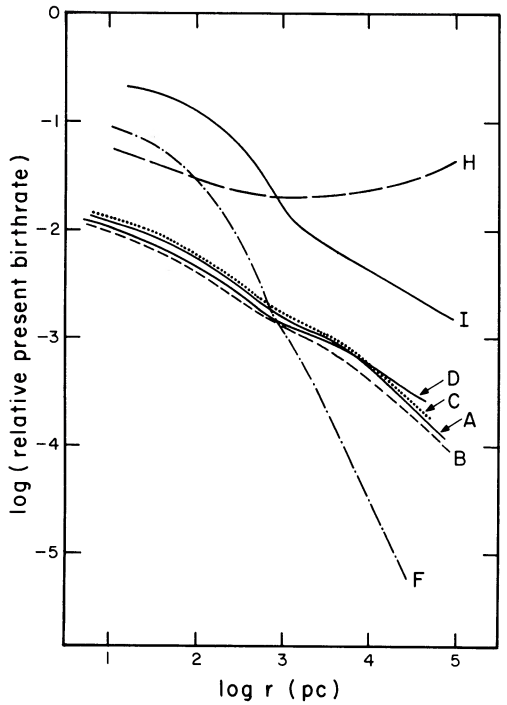

FIG. 2.—The relative present star formation rate versus radius in each model at age 11×10^9 yr. The quantity plotted is the ratio (density of stars formed between 10 and 11×10^9 yr)/(total density of stars present at 11×10^9 yr).

after the first 10^9 years. Its photometric properties are intermediate between those of the two single-burst models with $x = 1.0$ and $x = 1.5$ studied by Tinsley (1972*c*). In estimating the possible effect of a metal abundance gradient on the photometric properties, we have used the final metal abundances obtained for model B; this is legitimate since the final metal abundance distribution of model B is almost entirely established within the first 10^9 years.

III. PREDICTED PHOTOMETRIC PROPERTIES AT THE PRESENT EPOCH

a) UBV Colors

In table 1 we present results for the predicted broad-band colors $B - V$ and $U - B$ at several representative radii in each model. For computational reasons, these results are calculated for an assumed model age of 11×10^9 yr, rather than the 12×10^9 yr adopted in Paper I; however, this difference is unimportant compared with the uncertainties involved. The table gives the $B - V$ and $U - B$ colors computed assuming solar abundances for all stars, and also the estimated $B - V$ colors corrected for nonsolar composition as described in the Appendix. (The $U - B$ color cannot be corrected in the same way because of the lack of adequate fundamental data on line blanketing.) Computational inaccuracies may cause errors of 0.01–0.02 mag in the calculated colors, and uncertainties in the late stages of stellar evolution can also affect the colors by a comparable amount (Rose and Tinsley 1974).

The average stellar metal abundances $\langle Z_* \rangle$ used in estimating the color corrections in $B - V$ are also listed in table 1 for each zone; $\langle Z_* \rangle$ denotes the metal abundance averaged along a line of sight through the galaxy, and is the same as the "projected metal abundance" Z_p of Paper I. This average is presumably the best quantity to use in comparisons with observations, but its use here is not strictly consistent with the fact that the photometric properties have been computed only for individual spherical shells and not averaged along lines of sight. At present the labor required to average the photometric properties along lines of sight does not appear to be warranted; however, the effect would be to moderate somewhat the radial color gradients indicated by table 1 and figure 3, particularly at small radii where the light from the nucleus is diluted by the light of outlying regions seen projected in front of it.

The radial variation of the *UBV* colors of representative models is illustrated in figure 3. Results for models C and D are not shown since model C is intermediate between models A and B, and model D is nearly identical to model B. The uncorrected colors for the single-burst model S are independent of radius and are indicated by the circled dots at $U - B = 0.56$ and $B - V = 0.98$ on the right of the diagram. It is evident in figure 3 that in all cases (except model S) the uncorrected *UBV* colors, which are nearly uniform in the outer regions of each model, become significantly bluer in the nucleus ($r \lesssim 2$ kpc); this is particularly true of the $U - B$ color, which is most affected by young stars. (Note that the logarithmic radius scale makes the nuclear region appear relatively more extended in figure 3 than it would on the sky.) The blue nuclear colors are a consequence of the continuing infall of gas into the nucleus. Reference to figure 2 shows immediately that the radial color variations closely reflect the radial variation in the present star formation rate in each model.

The effect of correcting the $B - V$ colors for nonsolar metal abundances is shown in the bottom panel of figure 3. The increase in $\langle Z_* \rangle$ toward the center of each model makes the nuclear colors somewhat redder, owing to both a decrease in stellar effective temperatures and an increase in line blanketing, and this reduces the predicted color gradients. For model B, the corrected $B - V$ is nearly constant throughout the system, and the very small remaining region of slightly bluer color at the center might well be undetectable observationally. However, model F, in which star formation is more centrally concentrated, still shows a conspicuously blue nucleus. Model S, which represents a galaxy without recent star formation, has a $B - V$ color which becomes *redder* toward the center, reflecting only the metal abundance gradient. Thus, the nucleus of a galaxy can be either redder or bluer than the outer regions, depending on whether star formation is still going on in the galaxy and on how strongly it is concentrated toward the center.

Observations of color gradients in elliptical galaxies show that in most cases the nucleus is *redder* than the outer regions (e.g., de Vaucouleurs 1961; Miller and

TABLE 1

PROPERTIES OF THE MODELS AT AGE 11 × 10^9 YEARS

MODEL	RADIUS (pc)	M/L_B (solar units)	$\langle Z_* \rangle$	COLORS FOR SOLAR COMPOSITION		COMPOSITION-CORRECTED
				$U-B$	$B-V$	$B-V$
A.....	8.8	8	0.086	0.03	0.71	0.74
	70	11	0.057	0.17	0.79	0.83
	560	15	0.026	0.37	0.89	0.90
	4500	16	0.011	0.46	0.93	0.90
	18,000	17	0.011	0.51	0.95	0.91
B.....	8.8	13	0.103	0.19	0.80	0.85
	70	16	0.067	0.31	0.87	0.93
	560	20	0.030	0.45	0.93	0.95
	4500	20	0.014	0.51	0.96	0.94
	18,000	21	0.013	0.54	0.97	0.95
C.....	8.8	7	0.140	0.14	0.76	0.81
	70	10	0.092	0.26	0.84	0.86
	560	12	0.043	0.42	0.92	0.96
	4500	14	0.109	0.49	0.95	0.95
	18,000	14	0.018	0.54	0.96	0.95
D.....	10	12	0.103	0.19	0.79	0.81
	83	14	0.066	0.32	0.86	0.91
	660	17	0.031	0.45	0.93	0.95
	5300	19	0.013	0.50	0.95	0.92
	21,000	20	0.011	0.52	0.96	0.93
F.....	10	3	0.101	−0.17	0.48	0.51
	83	6	0.070	−0.05	0.62	0.65
	660	16	0.034	+0.43	0.92	0.95
	5300	19	0.010	+0.54	0.96	0.91
	21,000	20	0.004	+0.55	0.97	0.86
H.....	21	5	0.122	−0.07	0.59	0.62
	170	7	0.077	+0.02	0.66	0.70
	1400	9	0.040	+0.08	0.71	0.73
	11,000	8	0.018	+0.05	0.69	0.69
	44,000	7	0.008	−0.01	0.65	0.63
I.....	19	2	0.107	−0.25	0.39	0.43
	150	3	0.074	−0.17	0.49	0.52
	1200	9	0.038	+0.15	0.75	0.77
	9900	14	0.016	+0.34	0.87	0.86
	39,000	18	0.010	+0.41	0.91	0.86
S.....	8.8	22	0.103	0.56	0.98	1.07
	70	22	0.067	0.56	0.98	1.05
	560	22	0.030	0.56	0.98	1.00
	4500	22	0.014	0.56	0.98	0.96
	18,000	22	0.013	0.56	0.98	0.95

Prendergast 1962; Tifft 1969). This is in disagreement with the predictions for all models in which there is continuing star formation; however, model S has approximately the correct colors and qualitatively the correct color gradient. (It is difficult to make a stronger statement because of the uncertainties involved, particularly the uncertainty in the effect of composition on the colors.) This result suggests that recent star formation has not occurred in most elliptical galaxies, and is consistent with the possibility that galactic winds may have expelled their residual gas at an earlier stage of evolution (§ II). Another possibility is that star formation in elliptical galaxies occurs not continuously but only in sporadic bursts (perhaps only when a sufficient amount of gas has been accumulated); if so, it might well be that most of the time no effects of star formation are detectable.

It should be noted that, while most elliptical galaxies have red nuclei, there are also some that show unusually blue nuclei and/or other clear signs of ongoing nuclear star formation (Tifft 1969; van den Bergh 1972; Hodge 1973). For example, the $B-V$ color of the elliptical galaxy NGC 205 varies from $\sim$0.8 in the outer regions to $\sim$0.5 at the center (Hodge 1973), a color gradient which is similar to that predicted for model F. Thus the variation in predicted color gradients between different models is comparable with the variation in observed color gradients among real elliptical galaxies.

For comparison with the mean integrated *UBV* colors of various types of galaxies, we have taken for each model the uncorrected *UBV* colors at a representative radius of 5 kpc enclosing approximately half of the total mass; at this radius the composition is roughly solar in most models, so the composition correction should not be large. These colors are plotted in a two-color diagram in figure 4, along with the mean observed colors of various types of galaxies as given by de Vaucouleurs and de Vaucouleurs (1972). A few (uncorrected) *UBV* colors for the inner regions of models F and I, which have higher rates of star formation, are also shown for comparison. The

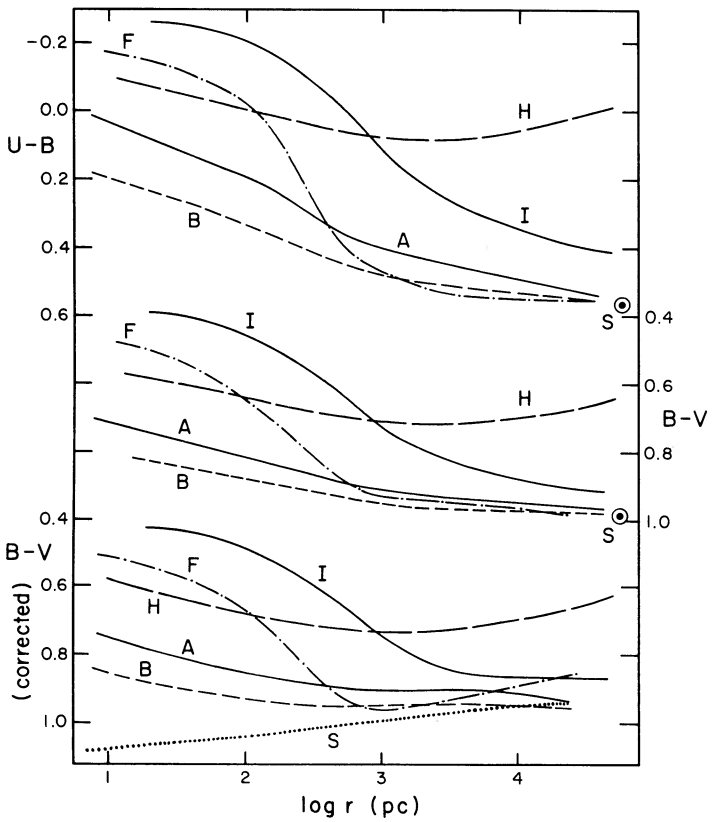

FIG. 3.—*UBV* colors versus radius in several representative models. The upper two panels show the colors uncorrected for composition; model S has colors independent of radius, indicated by the circled dots on the right. The bottom panel shows $B - V$ corrected for the composition gradient by the method described in the Appendix. Model S has the same composition as model B. All colors are for a model age of 11×10^9 yr.

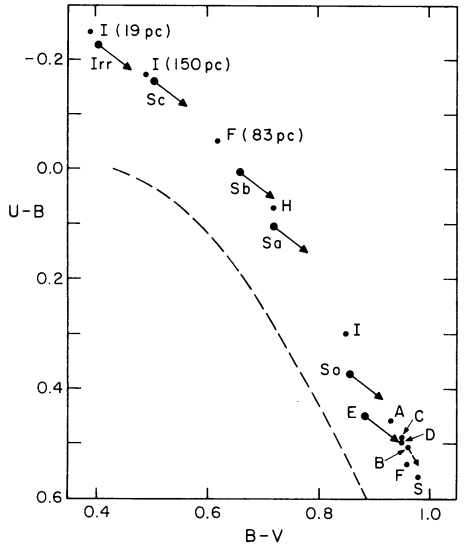

FIG. 4.—A two-color diagram showing the *UBV* colors of representative regions in the models (*dots*), the average colors of different types of galaxies (*large dots with arrows*), and the stellar main sequence (*dashed line*). Unless otherwise indicated, the model colors refer to a representative radius of 5 kpc and should be nearly the same as the integrated colors, as explained in the text. The arrows show the effect of removing a galactic reddening correction of $E(B - V) = 0.06$. The small dashed arrow for model B shows its evolution in 2×10^9 yr.

observed colors have been corrected for redshift, internal reddening, and reddening in our Galaxy, assuming $E(B - V) = 0.06$ at the galactic poles. Since some recent investigations (e.g., Sandage 1973) show little or no reddening at the galactic poles, arrows have been added in figure 4 to show the effect of removing a reddening correction of $E(B - V) = 0.06$ from the "observed" colors; this gives an indication of the uncertainty due to local reddening. An uncertainty is introduced into the predicted colors by the uncertainty in galactic ages; this is illustrated by the small dashed arrow for model B, which shows the effect of an age increase of 2×10^9 years (§ IV).

The model colors shown in figure 4 form a sequence in the two-color diagram which closely follows the sequence of observed galaxy colors. (The deviation of these colors from the stellar main sequence simply reflects the composite nature of galactic light.) In particular, it is noteworthy that models A–D and F, whose density profiles match those of elliptical galaxies, have *UBV* colors at $r = 5$ kpc that are very similar to the observed colors of elliptical galaxies, especially if there is no local reddening at the galactic poles. Since the composition-corrected colors of these models are almost constant outside the nucleus (see fig. 3), this agreement should apply also to the integrated colors, within the uncertainties caused by reddening and age effects.

Model H and the inner regions of models F and I have higher present rates of star formation (see fig. 2) and therefore, as might be expected, their *UBV* colors resemble those of spiral galaxies rather than ellipticals. We note, in fact, that the *UBV* colors of different regions of the models span the entire range of *UBV* colors observed for different Hubble types of galaxies. The agreement of *UBV* colors illustrated in figure 3 suggests that the star formation history of late-type spiral and irregular galaxies may be similar to that of the nuclear region of model I; it is not unreasonable that this should be the case, since, if rotation were present, the gas which falls into the nucleus of model I and forms stars there would instead condense into an extended disk like that of a spiral galaxy. In model I, continuing star formation is supported mainly by the infall of primordial gas from the outer part of the initial protocloud; thus the present results are consistent with the possibility that star formation in spiral galaxies may similarly be supported by the continuing infall of primordial gas (Larson 1972; Quirk and Tinsley 1973; Audouze and Tinsley 1974).

b) Mass-to-Luminosity Ratios

The computed mass-to-luminosity ratios M/L_B (in *B* light) are given in table 1 for several radii in each model. The comparison of these predicted M/L values with observations constitutes an important check on the models; unfortunately, however, the empirical M/L ratios of galaxies are still rather uncertain. Recent estimates give $M/L \sim (10\text{–}40)h$ for the central regions of elliptical galaxies (King and Minkowski 1972; Morton and Chevalier 1973) and $M/L \sim (1\text{–}13)h$ for spiral galaxies (Nordsiek 1973), where h is the Hubble constant in units of 100 km s^{-1} Mpc^{-1}; there appears to be a real range of values of M/L for each type of galaxy. Thus we see that models A–F have M/L values which, except in their nuclei, fall well within the range of values estimated for elliptical galaxies; model H and the nuclear regions of models F and I have M/L ratios characteristic of spiral galaxies. (In all of these regions only a negligible fraction of the mass is in the form of gas.) We note that these results are consistent with the comparison of *UBV* colors illustrated in figure 4, and they show that the major differences in M/L between different types of galaxies can, like the *UBV* colors, be accounted for in terms of different star formation histories, without involving large differences in the IMF.[1] Moreover, since both M/L and the average metal abundance of a model depend on the assumed IMF, it is noteworthy that the same simple choice of IMF gives approximately the correct results for both quantities; this consistency provides additional support for the present models.

The fact that the nuclei of models A–F have M/L ratios smaller than those usually estimated for elliptical galaxies is directly related to the fact that their colors are too blue; if the nuclear young star content were reduced enough to give colors in agreement with the observations for typical elliptical galaxies, the nuclear M/L values would become almost as large as those of the outer regions. Also, if the blue luminosity were corrected for composition effects, this would tend to reduce further the apparent gradient in M/L. Therefore it appears, within the uncertainties, that M/L may be nearly constant throughout any model whose colors match those of typical elliptical galaxies. This result justifies the assumption made in Paper I that it is valid to compare theoretical projected density distributions with the observed surface brightness distributions of elliptical galaxies. (We note, however, that there is no direct observational evidence, either from velocity dispersions or from rotation curves, that elliptical galaxies have nearly the same M/L at all radii, as these models would predict. Studies of the dynamics of clusters of galaxies suggest the possibility that the outermost regions of elliptical galaxies may have much larger M/L ratios than the inner bright regions [e.g., Rood *et al.* 1972; Oemler 1973].)

c) Continuum Spectral Energy Distributions

Absolute spectral energy distributions in the wavelength range between 0.33 and 1.1 μ have been calculated for the models in the manner described by Tinsley (1972*a*), using stellar data on the narrow-band scanner system of Spinrad and Taylor (1971). Figure 5 shows the results for the single burst model S, for model B at a representative radius of 4.5 kpc, for model H at 11 kpc, and for model I at 9.9 kpc. At these radii, $\langle Z_* \rangle \approx Z_\odot$ in each model; solar compositions have been assumed, since adequate corrections for other compositions cannot be made with existing data. Scans of the giant elliptical galaxy NGC 4889 (Gunn, private communication) and the Sc spiral M51 (Schild 1972) are also shown for comparison. No reddening correction has been applied, but the reddening should be small near the galactic poles. Models S and B agree well with the observations of NGC 4889, except at short wavelengths where they are slightly too blue; however, this discrepancy would be removed if the model ages were 1 or 2 $\times$ 10^9 years greater than the adopted 11 $\times$ 10^9 years (Tinsley 1972*c*; Rose and Tinsley 1974), or if the galaxy were slightly reddened. Model I is bluer than NGC 4889, as expected from its *UBV* colors, and model H closely resembles the Sc galaxy M51, in the limited wavelength range observed.

d) Spectral Features and Contributing Stellar Types

Table 2 gives the computed strengths of various spectral features as measured by the parameter w of Spinrad and Taylor (1969); w is a measure of the equivalent width of each feature. Also shown for comparison are the observed values of w for two old stellar populations in the inner regions of M31 and M32. Unfortunately there are no comparable data for giant elliptical galaxies or for the spiral-arm regions of

[1] A more detailed study of the relation between $B - V$ and M/L for different galaxies suggests, however, that the proportion of low-mass stars or "invisible mass" in the IMF may vary systematically with the type of galaxy (Sargent and Tinsley 1974). This effect does not appear to be large enough to alter significantly the present conclusions.

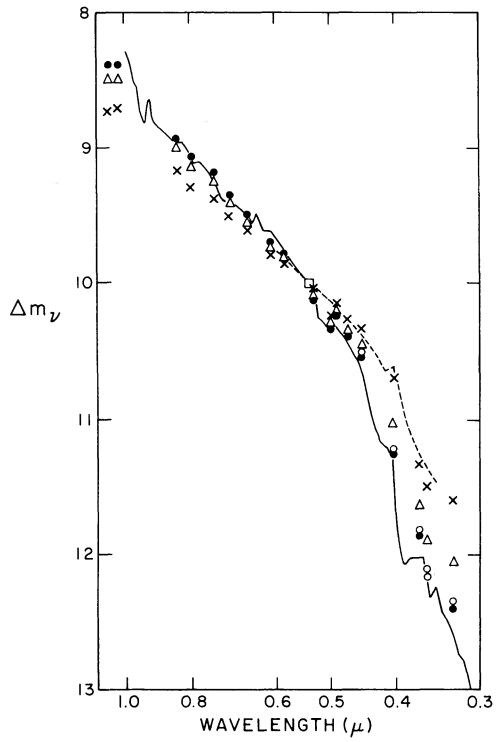

FIG. 5.—Continuum spectral energy distributions for several models and galaxies. The ordinate is $m_\nu = -2.5 \log f_\nu$ where f_ν is the flux per unit frequency interval, normalized to 10.00 mag at 5360 Å. The solid line is a scan of the giant elliptical galaxy NGC 4889 with bandwidths of 80 Å in the blue and 160 Å in the red (Gunn, private communication). The dashed curve is a scan of the Sc spiral galaxy M51 with a bandwidth of 100 Å (Schild 1972). Magnitudes for the models (at age 11×10^9 yr) are given at the continuum wavelengths of Spinrad and Taylor (1969, 1971) for radii where composition corrections should be small: model B at 4.5 kpc (*open circles*), model H at 11 kpc (*crosses*), model I at 9.9 kpc (*triangles*), and the single burst model S (*dots*). Model B is not shown separately if it differs from S by less than 0.01 mag.

spiral galaxies; however, the nuclear region of M31 appears to resemble an elliptical galaxy in most of its properties (Spinrad *et al.* 1971). From table 2, it is evident that models S and B closely resemble the observed old stellar populations in their line strengths, as they do in the continuum colors. An examination of the stellar birthrates for the various models (see fig. 2) shows that the contribution of early spectral types should increase in importance along the model sequence S, B, I, H, particularly at the shorter wavelengths. The feature strengths are consistent with this expectation: the neutral metal lines and the CN bands decrease in strength along the sequence, while the Balmer lines increase in strength, especially at short wavelengths; thus, for example, Hδ increases more strongly than Hα.

The fractional contribution of each spectral type to the total light in various wavelength bands can be determined from the computed distribution of stars in the H-R diagram. For models B and H, we show in table 3 the percentage of the light in the *U* band (0.36 μ), the *R* band (0.9 μ), and the *K* band (2.2 μ) contributed by stars in various regions of the H-R diagram.

For model B, it is seen that most of the light comes from the oldest stars, whose main-sequence turnoff at age 11×10^9 years is at spectral type G2. Dwarfs and subgiants near the turnoff provide most of the light in the *U* band, but at longer wavelengths the contribution of red giants becomes increasingly dominant. The relative contribution of giants and dwarfs to the red and infrared light depends on the slope of the IMF, and hence is closely related to the rate of evolution of the total luminosity, which is of cosmological importance (Sandage 1961; Tinsley 1972*a*, *b*, *c*, 1973). The relationship between the IMF and the relative contribution of giants and dwarfs is not significantly different from that found previously for the single burst models of Tinsley, since stars formed after the first 1 or 2×10^9 years are relatively unimportant in any region whose colors resemble elliptical galaxies. Thus the CO band at 2.3 μ, which measures the relative contribution of giant stars, should also be a sensitive indicator of the IMF, as discussed by Tinsley (1973).

The contribution table for model H reflects the presence of many more young early-type stars, especially in the *U* band, but even in this model the *K* light is dominated by red giants. Both models show an important contribution at all wavelengths from early K giants in the core-helium-burning stage of evolution, which form a "clump" near K1 III in the H-R

TABLE 2

STRENGTHS (*w*) OF SPECTRAL FEATURES IN MODELS AND GALAXIES

Feature	Wavelength (Å)	Dependence on Stellar Temperature	Dependence on Stellar Luminosity	Model S	Model B (4.5 kpc)	Model H (11 kpc)	Model I (9.9 kpc)	M31 Inner Disk*	M32 Nucleus†
Ca I.....	4227	negative	negative	0.19	0.18	0.08	0.14	0.17	0.13
G band (CH)	4300			0.30	0.29	0.18	0.25	0.29	0.28
Mg I + MgH	5175			0.24	0.24	0.18	0.21	0.26	0.19
Na I D.....	5892			0.10	0.10	0.07	0.09	0.08	0.08
Hδ.....	4100	strongest near A0 V	negative in early stars	−0.04	−0.02	0.19	0.07	−0.04	0.03
Hγ.....	4340			0.04	0.05	0.20	0.10	0.03	0.07
Hα.....	6564			0.17	0.18	0.21	0.19	0.16‡	0.20
CN.....	3880	negative	positive	0.33	0.31	0.13	0.24	0.26‡	0.27
CN.....	4200			0.15	0.14	0.05	0.11	0.14	0.13
CN.....	9200			−0.02	−0.01	0.00	−0.01	...	0.02

* Spinrad *et al.* 1971. † Spinrad and Taylor 1971. ‡ Affected by emission feature.

TABLE 3

CONTRIBUTIONS TO THE LIGHT (percent) IN DIFFERENT FILTER BANDS FROM STARS IN DIFFERENT REGIONS OF THE H-R DIAGRAM

Band	Luminosity Class	O	B	A	F	G0–4	G5–9	K0–4	K5–9	M0–4	M5–9
					Model B (4.5 kpc)						
U (0.36 μ).....	I, II	0.2	0.7	0.2	0.1	...	...	...	...	...	...
	III	...	...	...	...	...	0.2	11.7	0.4	1.0	0.4
	IV	...	...	0.1	0.2	0.4	12.8	6.0	...	...	...
	V	1.0	3.0	0.9	1.6	26.0	21.7	5.9	4.0	1.5	...
R (0.9 μ).....	I, II	...	...	...	...	...	...	0.1	...	...	...
	III	...	...	...	...	...	0.1	25.2	3.0	10.9	5.5
	IV	...	...	...	0.1	0.1	5.3	5.8	...	...	...
	V	...	0.2	0.1	0.4	9.4	9.0	6.1	9.9	7.6	0.7
K (2.2 μ).....	I, II	...	...	...	...	...	...	0.1	...	...	...
	III	...	...	...	...	...	0.1	14.0	2.9	21.9	30.8
	IV	...	...	...	...	...	1.3	2.3	...	...	...
	V	...	...	...	0.1	2.2	2.3	2.4	5.9	10.0	3.7
					Model H (11 kpc)						
U (0.36 μ).....	I, II	1.5	6.1	2.0	0.9	0.5	...	0.3	...	...	...
	III	...	0.2	0.1	...	...	1.5	5.0	0.2	0.6	0.1
	IV	...	0.2	0.5	1.9	3.0	0.7	1.9	...	...	...
	V	8.2	25.4	7.4	15.7	9.6	3.5	1.4	1.0	0.4	...
R (0.9 μ).....	I, II	...	0.5	0.6	0.5	0.6	...	1.9	0.1	0.6	...
	III	...	...	...	...	...	2.8	25.3	2.4	12.6	3.8
	IV	...	...	0.2	1.1	2.4	0.7	4.1	...	...	...
	V	0.5	3.1	2.4	9.0	7.4	3.7	3.3	5.4	4.2	0.4
K (2.2 μ).....	I, II	...	...	0.1	0.1	0.2	...	1.2	0.1	1.0	...
	III	...	...	...	...	...	1.3	17.3	2.7	27.6	24.9
	IV	...	...	...	0.3	0.7	0.2	1.9	...	...	...
	V	...	0.3	0.4	2.2	2.0	1.2	1.6	3.8	6.5	2.4

diagrams of old clusters and moving groups (Cannon 1970).

e) Ultraviolet Fluxes

In order to study the young stellar content of galaxies and compare it with model predictions, it is particularly useful to have observations at ultraviolet wavelengths, where the young stars show up most prominently. Such observations have recently been made by the OAO-2 satellite, and preliminary results have been described by Code, Welch, and Page (1972). We have computed ultraviolet fluxes for the present models at the OAO-2 wavelengths of 1910, 2460, 2980, and 3320 Å, using where possible stellar data on the same broad-band filter system; the data of Doherty (1972) have been used for stars with $B - V > 0$, and the model atmospheres of van Citters and Morton (1970) have been used for hotter stars. The resulting ultraviolet fluxes, supplemented by fluxes at the *UBV* wavelengths and normalized to unity at 3320 Å, are plotted in figure 6 for a number of representative regions in the models. The OAO-2 observations of the nuclear and spiral arm regions of M31 (Code *et al.* 1972) are also shown for comparison.

As expected, the ultraviolet flux is seen to be a sensitive indicator of the present star formation rate, particularly at wavelengths shorter than $\sim$2500 Å where the hot young stars (if present) cause an upturn in the spectral energy distribution. Regions with low present rates of star formation, such as the outer part of model D ($r \gtrsim 5$ kpc), have low ultraviolet fluxes similar to that observed in the nucleus of M31; regions with intermediate rates of star formation, such as model H and the inner part of model F ($r \lesssim 500$ pc), resemble the spiral-arm region of M31; and regions with high rates of star formation, such as the nucleus of model I, have even larger ultraviolet fluxes resembling those observed in late-type spiral and irregular galaxies (Code *et al.* 1972). These results are consistent with the comparisons of *UBV* colors illustrated in figure 4. However, close agreement with the observations cannot be expected here because of our neglect of interstellar absorption, composition effects, and possible contributions from hot horizontal branch stars. (The possible contribution of hot pre–white-dwarf stars to the ultraviolet light has been shown by Rose and Tinsley (1974) to be unimportant at wavelengths greater than 2000 Å.)

Ultraviolet observations of elliptical galaxies will be of value in establishing whether they contain any young stars. The preliminary OAO-2 results for elliptical galaxies (Code *et al.* 1972) show an upturn at short wavelengths similar to that observed for spiral galaxies, which if real could indicate the presence of a young stellar component. However, a quantitative comparison of the present results with observations of elliptical galaxies must await the revised reduction of the OAO-2 results (Welch, private communication).

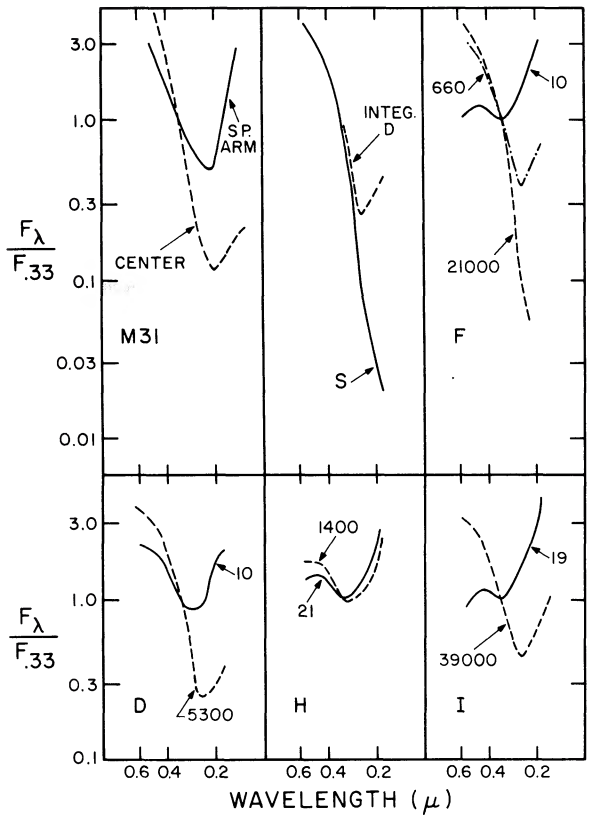

FIG. 6.—Ultraviolet spectral energy distributions, given in terms of flux per unit wavelength interval and normalized to unity at 3320 Å. The upper left panel shows observed data for M31, taken from Code *et al.* (1972). The top central panel shows the spectrum of model S, which has no young stars, and the integrated spectrum of model D estimated on the basis of the total present star formation rate. Other panels give results for models F, D, H, I at the radii indicated in parsecs. Models A, B, and C are all very similar to model D.

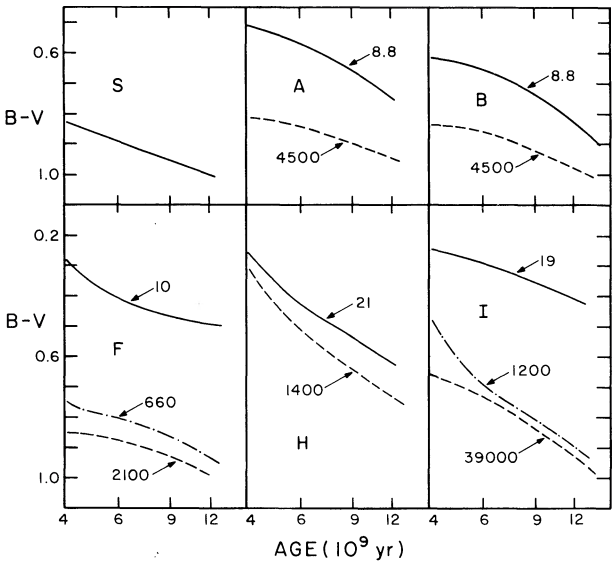

FIG. 7.—The evolution of $B - V$ (not corrected for composition) in several models at the radii indicated in parsecs.

IV. EVOLUTION OF THE PHOTOMETRIC PROPERTIES

In order to understand the properties of elliptical galaxies observed at large redshifts and use them for cosmological purposes, it is necessary to know how their photometric properties evolve with time. In this section we give some results for the photometric evolution of the models at times after $t = 4 \times 10^9$ years, corresponding to redshifts less than about 1. We have not attempted to predict the photometric properties at earlier times, since the lack of adequate data on late stages of stellar evolution makes such calculations unreliable. (Note, however, that the luminosity of a galaxy during the earliest stages of its evolution can be estimated as being approximately proportional to the total star formation rate, as described in Paper I.) The calculations have here been carried up to $t = 12 \times 10^9$ years.

a) Evolution in Color

The evolution of the (uncorrected) $B - V$ colors of several representative regions of the models is illustrated in figure 7. As expected, all regions become redder with time, owing mainly to the evolution toward redder colors of the main-sequence turnoff point of the oldest stellar populations, which generally contribute most of the light. In regions where continuing star formation is important, as in model H, the decreasing rate of star formation also contributes to the redward color evolution because of the decrease in the number of young blue stars present.

The present rate of color evolution for the regions whose colors match those of elliptical galaxies—i.e., the nonnuclear regions of models A–F and model S—can be compared with the rate of color evolution derived from observations of elliptical galaxies at different redshifts. Oke and Sandage (1968) found that $B - V$ varies by less than 0.03 mag for redshifts up to $z = 0.2$; this corresponds to a look-back time of approximately $1.6 \times 10^9 h^{-1}$ years, where h is the Hubble constant in units of 100 km s^{-1} Mpc^{-1}. Hence the present rate of change of $B - V$ is less than about $0.02h$ mag per 10^9 years. The predicted rates of change of $B - V$ for the models are difficult to calculate accurately, but values between approximately 0.01 and 0.02 mag per 10^9 years are found for the outer regions of models A–F and for model S. These values are consistent with the observed upper limit if $h = 1$, although there is possibly a discrepancy in some cases if $h = 0.5$.

A more stringent test of the models can be made by comparing the model predictions with Oke's (1971) spectral scans of elliptical galaxies at large redshifts. Figure 8 shows the observed spectral energy distribution (corrected to zero redshift) of 3C 295, which has a redshift of $z = 0.46$ corresponding to a look-back time of about $3 \times 10^9 h^{-1}$ years. Also shown are the predicted continuum intensities of model B ($r = 4.5$ kpc) and model S at an age of 5×10^9 years, corresponding to a present time of 11×10^9 years and a

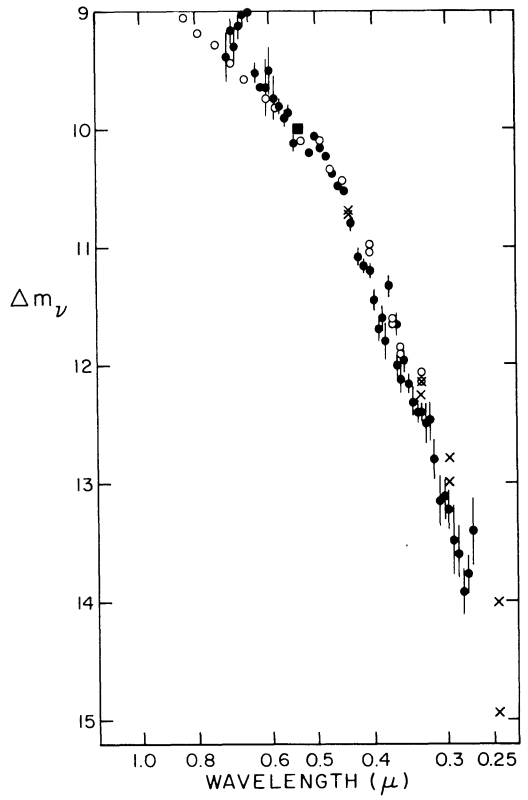

FIG. 8.—Spectral energy distributions of relatively young systems, plotted as in fig. 5. The dots with error bars are data for 3C 295 (Oke 1971), corrected for the redshift of $z = 0.46$ to give the rest wavelength as abscissa. (The high flux at 3727 Å is due to gaseous emission and should be disregarded.) Results for models B and S at age 5×10^9 yr are also shown, as derived from the Spinrad-Taylor continuum points (*open circles*) and the ultraviolet fluxes at the OAO-2 wavelengths (*crosses*); the results for the two models are shown separately only where they differ by more than 0.01 mag, and model B always has the greater flux (*bluer color*).

look-back time of 6×10^9 years, as applicable if $h = 0.5$. As remarked by Oke (1971), the spectral energy distribution of 3C 295 is not noticeably different from that of galaxies with much smaller redshifts. Model B, however, evolves appreciably during the look-back time, and at age 5×10^9 years it is bluer at short wavelengths than 3C 295. This is largely due to the young stars present in model B, as is evident from the fact that the agreement is better for model S, in which star formation is not taking place at 5×10^9 years. This result suggests that star formation in 3C 295 may have been cut off at a relatively early stage of evolution, i.e. before 5×10^9 years, but a strong statement cannot be made because of the observational uncertainties in the input data used to obtain the ultraviolet colors of the models (crosses in fig. 8) and in the spectral energy distribution of 3C 295.

b) Evolution in Luminosity

The evolution of galaxies in absolute magnitude M_V is important because the apparent magnitudes of distant elliptical galaxies must be corrected for evolution before the cosmological deceleration parameter q_0 can be determined. A lower limit to the effect of evolution on q_0 can be estimated from the following simple first-order formula which is valid at small redshifts:

$$\Delta q_0 = \frac{1}{H_0}\frac{dM_V}{dt} = \frac{1}{H_0 t}\frac{dM_V}{d\ln t} > \frac{1}{H_0 t_0}\frac{dM_V}{d\ln t} > \frac{dM_V}{d\ln t}, \quad (2)$$

where Δq_0 is the amount by which q_0 must be corrected downward if galaxies are growing fainter, H_0 is the present Hubble constant in inverse time units, t_0 is the present age of the Universe and t is the age of the galaxy at the time of observation. The first inequality in equation (2) holds because $t < t_0$, and the second one holds in Friedmann cosmologies with zero cosmological constant, in which $H_0 t_0 < 1$. Equation (2) applies approximately to both the value of q_0 derived from the magnitude-redshift relation (Tinsley 1972*b*) and the value obtained from the isophotal diameter-redshift relation (Tinsley 1972*d*).

Figure 9 shows the evolution of M_V at several radii in representative models, normalized such that $M_V = 0$ at $t = 10^{10}$ years. For model S and the nonnuclear regions of models B, C, D, and F, all of which have the same (Salpeter) IMF, the absolute magnitude evolves at the same nearly constant rate, $dM_V/d\ln t = 0.87$. Model A, which has a less steep IMF, evolves slightly faster, with $dM_V/d\ln t = 1.20$. These results are in

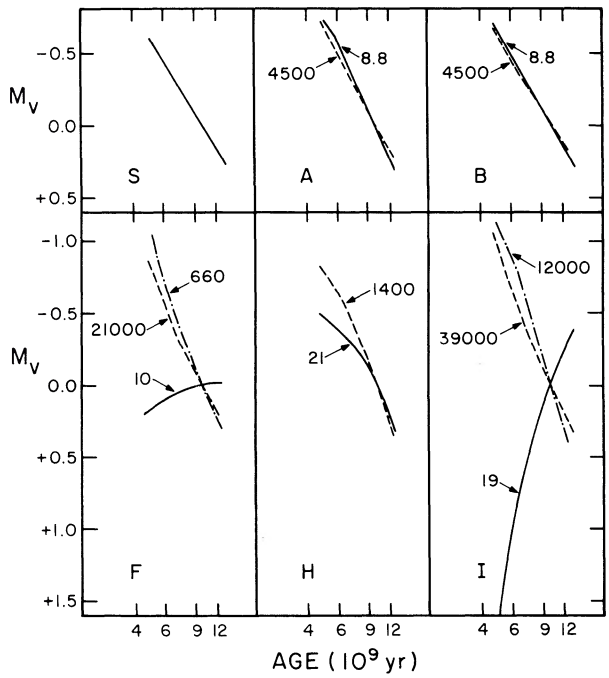

FIG. 9.—The evolution of the absolute magnitude M_v normalized to zero at age 10×10^9 yr for several models at the radii indicated in parsecs.

agreement with previous results for single burst models, which show that $dM_V/d\ln t$ depends strongly on the IMF but hardly at all on the age of the model or on uncertainties in stellar evolution (Tinsley 1972*c*; Rose and Tinsley 1974). The present results show in addition that the occurrence of continuing star formation in models A–F has a negligible effect on the rate of luminosity evolution; this is true even for the nuclei of models A–D, where the star formation rate is higher than allowed by the colors for normal elliptical galaxies. This can be understood from the fact that each generation of stars evolves approximately according to homology formulas and with almost the same value of $dM_V/d\ln t$, which depends only on the IMF (Wielen 1964; Tinsley 1972*b*). Thus we conclude that the present models indicate an evolutionary correction to q_0 of the order of $\Delta q_0 \sim 1$, and that this prediction is not appreciably affected by the possible occurrence of continuing star formation in elliptical galaxies at any rate allowed by the observations.

A further significant conclusion follows from the fact that $dM_V/d\ln t$ is very nearly independent of radius in models A–D. This means that the luminosity profiles of elliptical galaxies should not show any evolutionary changes in form out to redshifts of at least $z \sim 0.5$. Hence the aperture corrections derived by Sandage (1972) for nearby galaxies should also be applicable to galaxies at large redshifts, and the effect of variations in galaxy profiles is unimportant for the angular-diameter–redshift relation (Tinsley 1972*d*).

V. THE SUPERNOVA RATE IN GALAXIES

Tammann (1974) has recently discussed the statistics of supernovae in different types of galaxies and has made new estimates of the supernova rate per unit galactic mass in galaxies of different Hubble types. As discussed by Tammann, there are reasons to believe that all supernovae, not just the Type II supernovae, belong to a young stellar population and result from the demise of massive short-lived stars. If so, the supernova rate in a galaxy is simply proportional to the total star formation rate. Hence the supernova rate can be predicted for any model or region whose present star formation rate is known, given the IMF and some assumption as to which stars become supernovae. In order to obtain such predictions for the present models we shall assume, following Gunn and Ostriker (1970), that all stars more massive than 4 $M_\odot$ become supernovae; then the constant of proportionality relating the supernova rate (in supernova events per 100 years) to the star formation rate (in solar masses per year) is 1.26 for the IMF of model A, 1.05 for the IMF of model B, and 1.36 for the IMF of model C. To give an indication of the uncertainty in these predictions, we consider also the possibility that only stars more massive than 6 $M_\odot$ become supernovae; the above constants of proportionality then become 0.63 for model A, 0.59 for model B, and 0.77 for model C. A lower mass limit of 6 $M_\odot$ is suggested by the probable existence of a white dwarf in the Pleiades cluster, which has a turnoff mass near 6 $M_\odot$ (Trimble and Greenstein 1972; Woolf 1974).

In order to predict the supernova rates to be expected in galaxies of different Hubble types, it is necessary to estimate the total present rate of star formation per unit galactic mass in each type of galaxy. From the results of § III (cf. also Searle, Sargent, and Bagnuolo 1973) it is clear that the *UBV* colors of a model galaxy with a given IMF depend closely on the present star formation rate; hence it is possible to estimate the star formation rate in a galaxy from a knowledge of its *UBV* colors. To make this estimate, we have used the star formation rates illustrated in figure 2, together with the *UBV* colors given in table 1 for different regions of the models, to prepare a plot showing the dependence of $U - B$ and $B - V$ on the present relative star formation rate; the resulting curves are the same for all regions of models B–I, but are somewhat different for model A owing to the different form of the IMF (fig. 1 of Paper I). From this plot it is possible to read, for any of the assumed IMFs, the present relative star formation rate in a galaxy whose *UBV* colors are given. Adopting the mean *UBV* colors indicated by the arrows in figure 4 for galaxies of different Hubble types, we obtain in this way the estimated star formation rates listed in table 4 in units of solar masses per year 10^{11} $M_\odot$ total galactic mass. Multiplying by the factors given in the preceding paragraph, we then obtain the predicted supernova rates shown in table 4 in units of supernovae per 100 years per 10^{11} $M_\odot$ total galactic mass. Finally, the observed supernova rates are given in the same units, as obtained directly from table X of Tammann (1974). In case the arguments that all types of supernovae come from massive stars are incorrect and only the Type II supernovae descend from massive stars, as traditionally believed, we have listed also the rates for Type II supernovae alone, obtained from the data of Tammann (1974) by assuming that one-third of the unclassified supernovae are of Type II.

Considering that both the predicted and the observed supernova rates are quite imprecise, the agreement obtained in table 4 is very good, especially for the IMF of model B. The only significant discrepancy between predicted and observed supernova rates occurs for the irregular galaxies, which have an unexplained apparent deficiency of supernovae (Tammann 1974). The generally good agreement (perhaps fortuitously close) between the predicted and observed supernova rates provides further reassuring support for the various relatively conventional assumptions adopted in the present models, In particular, we can conclude that the observed supernova rates in galaxies are consistent with the assumption that supernovae result from the deaths of stars more massive than 4 $M_\odot$. If only the Type II supernovae are considered, the data in table 4 are equally consistent with the assumption that the Type II supernovae come from stars more massive than 6 $M_\odot$, except that the discrepancy for irregular galaxies becomes worse because of the absence of any observed Type II supernovae in these systems. Sargent, Searle, and Kowal (1974) also obtained satisfactory agreement

TABLE 4

PREDICTED STAR FORMATION AND SUPERNOVA RATES FOR IMF's A, B, C, AND LOWER MASS LIMIT 4 $M_\odot$ (6 $M_\odot$)

GALAXY TYPE	STAR FORMATION RATE [$M_\odot$ per year per 10^{11} $M_\odot$]			PREDICTED SUPERNOVA RATES [SN per 100 years per 10^{11} $M_\odot$]			OBSERVED SUPERNOVA RATES	
	A	B	C	A	B	C	All Types	Type II
E	$\lesssim 0.05$	$\lesssim 0.1$	$\lesssim 0.1$	$\lesssim 0.06(0.03)$	$\lesssim 0.1(0.06)$	$\lesssim 0.1(0.1)$	0.07	0
S0	0.13	0.2	0.2	0.2(0.1)	0.2(0.1)	0.3(0.2)		
Sa	0.6	1.1	1.1	0.8(0.4)	1.2(0.6)	1.5(0.8)	0.8	0
Sb	1.1	2.0	2.0	1.4(0.7)	2.1(1.2)	2.7(1.5)	1.9	1.0
Sc	3.0	5.5	5.5	3.8(1.9)	5.8(3.2)	7.5(4.2)	5.7	3.1
Ir I	5	9	9	6 (3)	9 (5)	12 (7)	3.8	0

between the observed Type II supernova rates in galaxies with different *UBV* colors and the relative supernova rates predicted on the basis of theoretical stellar birthrates.

The observed supernova rate of ~ 0.07 SN per 100 years per 10^{11} $M_\odot$ in elliptical and S0 galaxies is almost the same as the rate of ~ 0.1 SN per 100 years per 10^{11} $M_\odot$ predicted for models A–F, in which the present star formation rate is ~ 0.1 $M_\odot$ per year (fig. 1); this agreement is consistent with Tammann's (1974) suggestion that the supernovae in elliptical galaxies reflect a finite, although small, current rate of star formation. As we have seen, the integrated *UBV* colors of elliptical galaxies are consistent with the predicted star formation rates in models A–F, but within the uncertainties they are also consistent with no present star formation at all, and thus do not indicate whether or not star formation is occurring at the low rate of ~ 0.1 $M_\odot$ per year required to explain the observed supernova rate. The absence in most elliptical galaxies of the bluer nuclei predicted by the models suggests, as discussed in § III, that star formation at this rate is not taking place in most elliptical galaxies. However, it is worth recalling that some elliptical galaxies do show blue nuclei and/or other signs of current star formation, and they should therefore produce supernovae at a significant rate. Unfortunately, little appears to be known about most of the elliptical galaxies in which supernovae have been discovered, but it would clearly be of interest to determine whether any of them show any other signs of current or recent star formation.

Traditionally, the view that Type I supernovae belong to an old stellar population and come from stars of mass ~ 1 $M_\odot$ has been based on the assumption that elliptical galaxies, which apparently produce only Type I supernovae, contain no young stars. In view of the above results this argument no longer seems compelling, since elliptical galaxies could contain enough young stars to account for the low observed supernova rate, provided that the young stars are not too concentrated at the center or, as seems more likely, if only some elliptical galaxies contain young stars and produce supernovae. Thus our results add some plausibility to Tammann's (1974) suggestion that Type I supernovae actually come from relatively massive young stars.

VI. CONCLUSIONS

In general, the integrated photometric properties of models A–F at ages ~ 11–12×10^9 years are in good agreement with the observed photometric properties of elliptical galaxies; this goes for the *UBV* colors ($B - V \sim 0.95$, $U - B \sim 0.50$), the mass-to-luminosity ratios ($M/L \sim 20$), the continuum spectral energy distributions, and the spectral line indices, all of which agree within the uncertainties involved. Since both the photometric properties and the average metal abundance of a model depend primarily on the assumed initial mass function, it is significant that approximately correct results for both are obtained with the same conventional choice of IMF, which is similar to that of the solar neighborhood (and is invariant in space and time). Thus it is possible to reproduce satisfactorily many, if not all, of the integrated photometric properties of elliptical galaxies on the basis of the simple and relatively conventional models and assumptions described in Paper I and the present paper.

In models A–F, whose properties closely resemble those of elliptical galaxies, nearly all of the star formation is completed during the first $\sim 2 \times 10^9$ years, and the low residual rate of star formation present after ~ 11 or 12×10^9 years makes no important difference to any of the integrated photometric properties, which are very similar to those of a single burst model (except at ultraviolet wavelengths $\lesssim 2500$ Å). However, the tendency of the residual star formation activity to become concentrated at the center makes the nuclei of these models look somewhat bluer than the outer regions, in contraction to the observations which show that most elliptical galaxies have redder nuclei. This result suggests that most elliptical galaxies do not even have the low present rates of star formation predicted by the models; probably this is because they have earlier lost their residual gas, either through expulsion by an internal energy source or possibly through being swept clean by an "intergalactic wind" (Gunn and Gott 1972). The fact that model B appears to be bluer than 3C 295 at age 5×10^9 years suggests that gas loss in 3C 295 occurred before this time.

As far as the evolution of the photometric properties is concerned, the present results show that the possible occurrence of continuing star formation in an elliptical galaxy has only a small effect on the evolution of its

UBV colors, and no appreciable effect on its evolution in luminosity. Thus, even if continuing star formation does occur, it is not likely to alter any of the conclusions previously obtained for single burst models. In particular, it still appears likely that elliptical galaxies become fainter with time at a rate sufficient to require a significant downward correction to the cosmological deceleration parameter.

In regions where star formation remains important after 12×10^9 years, particularly in the "expanding models" H and I, the predicted photometric properties resemble those of spiral rather than elliptical galaxies; in fact, different regions in the models exhibit the whole range of *UBV* colors observed for different Hubble types of galaxies. The mass-to-luminosity ratios are consistent with the *UBV* colors in that the regions whose *UBV* colors resemble spiral galaxies also have M/L ratios characteristic of spiral galaxies. The fact that these results are obtained with the same IMF which was found to reproduce well the properties of elliptical galaxies suggests that approximately the same "universal" IMF may be applicable to all types of galaxies; the present model results show that most of the differences in photometric properties and mass-to-luminosity ratios between different types of galaxies can be accounted for simply as a consequence of different star formation histories (cf. also Searle *et al.* 1973).

We recall that in Paper I it was found to be possible to explain the observed distribution of stellar metal abundances as being a result of the dynamical evolution of a galaxy, without invoking variations in the IMF as had previously been customary. In the present paper we have found that a similarly simple explanation in terms of differences in the star formation history is able to account for many of the variations in photometric properties within and between galaxies, again without invoking substantial variations in the IMF. Thus a principal conclusion of the present project is that many of the basic properties of different types of galaxies can be explained on the basis of quite simple assumptions if the dynamical consequences of a conventional collapse picture of galaxy formation are followed through with detailed calculations.

It is a pleasure to thank Dr. R. A. Bell for valuable discussions of the effects of metal abundance on color, and Drs. J. E. Gunn, G. A. Welch, and G. A. Tammann for providing unpublished data. B. M. T.'s work has been supported in part by NSF grants GP-30455X and GP-40482, and by the Center for Theoretical Physics of the University of Maryland during six months of 1973.

APPENDIX

THE DEPENDENCE OF STELLAR COLOR ON METAL ABUNDANCE

I. LIMITATIONS AND OUTLINE

The program of Tinsley (1972*a*) for computing the photometric properties of a region with a given stellar birthrate incorporates theoretical stellar evolutionary tracks for solar-composition stars; semiempirical tracks derived from old clusters and groups of about solar composition; and calibrating relations between effective temperature, bolometric correction, spectral type, and color derived for "normal" Population I stars. The properties calculated should therefore be valid for a region in which the mean stellar metal abundance $\langle Z_* \rangle$ is about solar and the dispersion of Z values is not too great. For other regions, the ideal method of obtaining photometric properties would be to use different stellar input data according to the value of Z for each star. Since not enough is known empirically or theoretically to use this method with a useful degree of reliability, we adopt the following alternative. Colors of all regions are computed as though every star had solar composition, and then differential corrections are made as though every star in the region had the average metal abundance $\langle Z_* \rangle$. Possible variations in relative abundances among the elements heavier than ^{4}He (e.g., variations in the C/Fe ratio) are ignored, although these are known to occur (Hearnshaw 1972) and will affect stellar evolution and line blanketing in a way not represented by the single parameter Z. The unlikely possibility of significant variations in the helium abundance is also ignored. We take $Z_\odot = 0.02$.

Three effects must be considered for each star:

a) The "lifetime effect," whereby stellar structural effects cause the main-sequence lifetime of a star of given mass to increase with Z. If we consider the generation of stars formed during a specified time interval, say between 1 and 2×10^9 years, these stars evolve through stages like successively older clusters. The turnoff mass of the generation at a given later time increases with Z, so the generation tends to have *bluer* colors at greater Z.

b) The "structural effect," whereby the effect of Z on stellar interiors and atmospheres causes the effective temperature and bolometric luminosity of a star of given mass at a given evolutionary stage to depend on Z.

c) The "blanketing effect," whereby the colors of a given T_e and evolutionary stage depend on Z through blocking and back-warming. Effects (*b*) and (*c*) were considered by Faber (1973) in her estimates of composition effects on populations with the same distribution of stellar *masses*. Each of these effects makes a population of greater Z redder. Since we are interested in a given distribution of stellar *ages*, we must include effect, (*a*), which has the opposite effect on the colors.

Because of the paucity of essential data, especially on blanketing at the shortest and longest wavelengths and in stars cooler than early K, we attempt to find the correction only to $B - V$.

II. THE LIFETIME EFFECT

Consider the generation of stars formed with metal abundance Z at time t_f, and seen now at time t. Its turnoff mass at time t is the same as that of a hypothetical generation with abundance $Z_\odot$ at time t_m, where

$$\frac{t_m - t_f}{t - t_f} = \left[\frac{Z + 0.012}{Z_\odot + 0.012}\right]^{-0.28}. \quad (3)$$

Equation (3) is derived from Sandage and Eggen's (1969) estimate of the lifetime effect, using the evolutionary tracks of Aizenman, Demarque, and Miller (1969). It implies that the distribution of stellar masses and evolutionary stages is the same at time t in the generation with abundance Z as it is at time t_m in the generation with abundance $Z_\odot$. This distribution can therefore be obtained by using our standard program, evolving the generation to time t_m rather than t.

If the stars in a galaxy were coeval, as in a single-burst model, it would be no problem to make the lifetime correction. One would use the computed population at time t_m, and correct its stars for the other effects to obtain the colors that would be found at time t with metal abundance Z. With a spread in times of star formation, one could follow this procedure separately for the stars formed in 10^9 year intervals and sum the resulting properties. However, it appears in nearly all regions of the present models that the B and V light is dominated by stars formed in a small time interval, for example the first 10^9 years in the outer regions of model B and the last 10^9 years in the nucleus of model I. We therefore use a simpler procedure that does sufficient justice to the accuracy of the other two corrections: a single value of t_f is adopted for each region, based on the formation time of the stars contributing most of the B and V light. The uncertainty introduced in the final colors is generally $\lesssim 0.01$ mag, and at most 0.03 mag in the nuclear region.

III. THE STRUCTURAL EFFECT

To determine the effect of Z on T_e and L_{bol} for a star of given mass and evolutionary stage, it is essential to use stellar evolutionary tracks computed with the same code and input physics; otherwise extraneous effects may dominate. For main-sequence stars, the models of Copeland, Jensen, and Jørgensen (1970) have been used; and for subgiants and giants, the models of Torres-Peimbert (1971) have been used. The latter cover only a small range of stellar mass, but they include the masses most important for $B - V$ in old populations. For lack of more detailed information, it has to be assumed that the changes $\Delta \log T_e$ and $\Delta \log L_{bol}$ are proportional to $\Delta \log Z = \log (Z/Z_\odot)$ in the interval of interest, i.e., $-0.7 \lesssim \Delta \log Z \lesssim +0.7$.

To apply the structural correction to a region, we start with the distribution of stars in the theoretical H-R diagram that is obtained after application of the lifetime correction. Each star is then moved by the appropriate $\Delta \log T_e$ and $\Delta \log L_{bol}$ to a new position. "First revised" values of $B - V$, M_V, and the bolometric correction (BC) for each star are then derived for its new position. Tables of $B - V$ and BC based on data for "normal" stars have been used for this purpose, but this should be adequate since the blanketing effects are treated separately.

IV. THE BLANKETING EFFECT

It is now necessary to obtain the effect of blanketing on $B - V$, given $\log T_e$. (Blanketing effects on luminosity can be neglected relative to the structural effects.) Unfortunately, reliably calibrated data are available only for a very limited region of the H-R diagram, so considerable extrapolation and guesswork are necessary.

For F and G dwarfs, we adopt the differential color corrections determined by Bell (1971) from synthetic spectra, which appear to be very reliable (Branch and Alexander 1973). These are extended to hotter stars by extrapolation of the relation between $b = \Delta(B - V)/\Delta \log Z$ and $R - I$ to zero for stars with $R - I < 0$, and to cooler stars by extrapolation at constant b for $R - I > 0.40$. (Luckily, dwarf stars later than G8 are not important for $B - V$.) Positive and negative values of $\Delta \log Z$ are treated separately, since their values of b differ significantly.

In the case of giant stars, the lack of data is a serious problem. The following scheme gives results that are plausible because they are consistent with the dwarf data, but it is to be hoped that more reliably calibrated corrections will be available in the future. The abundances derived for many early K giants by Gottlieb and Bell (1972) are used in conjunction with the observed $B - V$ of each star and the standard $B - V$ for its $R - I$ (which should be a good temperature index, independent of blanketing) to obtain a plot of $\Delta(B - V)$ versus $\Delta \log Z$. This plot shows an unsatisfactory scatter, but the mean ratios $b = \Delta(B - V)/\Delta \log Z$, for positive and negative $\Delta \log Z$, can be fitted smoothly to the $(b, R - I)$-relationship for dwarfs. For giants later than those in Gottlieb and Bell's sample, it has been assumed that b is independent of $R - I$. This assumption may underestimate the blanketing in late giants, but will not cause significant error in the models since later giants are not important in B and V light.

The adopted b-values are used to revise further the color of each star, according to its luminosity class and structurally corrected $\log T_e$.

V. RESULTS

Table 5 illustrates the above procedure as applied to models D and I. Line 3 gives the color computed for each region at age 12×10^9 years, using standard (solar composition) data on stellar evolution and colors. Line 4 gives the mean stellar Z value for which these colors are to be corrected. Line 5 gives the time at which the star formation rate is greatest; this can also be seen from contribution tables in B and V (not given here) to be the formation time of those stars that

TABLE 5

SAMPLE CORRECTIONS OF $B - V$ FOR COMPOSITION

	D					I				
1. Model										
2. Radius (pc)	10	83	660	5300	21,000	19	150	1200	9900	39,000
3. Uncorrected color at age 12×10^9 yr, assuming $Z = Z_\odot$	0.80	0.87	0.94	0.97	0.98	0.41	0.52	0.79	0.90	0.93
4. Mean stellar Z, $\langle Z_* \rangle$	0.103	0.066	0.031	0.013	0.0113	0.107	0.074	0.038	0.0159	0.0097
5. Time of maximum star formation rate, t_f (10^9 yr)	1.2	1.2	1.2	1.2	1.3	12	~7	3.5	2.0	1.6
6. Model age for lifetime correction, t_m (10^9 yr)	8.8	9.6	11.1	12.8	13.0	12	~11	11.0	12.4	13.2
7. Corrected color, all effects	0.82	0.92	0.96	0.94	0.95	0.45	0.52	0.79	0.89	0.90
8. Color at age 12×10^9 yr, lifetime correction omitted	0.90	0.96	0.98	0.93	0.93	0.45	0.56	0.82	0.88	0.87
9. Best estimate for corrected color at age 12×10^9 yr	0.82	9.92	0.96	0.94	0.95	0.45	0.55	0.81	0.89	0.89
10. Correction (line 9 minus line 3)	+0.02	+0.05	+0.02	−0.03	−0.03	+0.04	+0.03	+0.02	−0.01	−0.04

contribute dominantly to the light in these bands. In model D, t_f is well defined (cf. fig. 5 of Paper I), but in model I star formation is much more uniform (cf. fig. 17 of Paper I) and this leads to a greater uncertainty in the lifetime correction. Line 6 gives the time t_m defined by equation (3) at which a population of composition $Z_\odot$ has the same distribution of stellar masses and evolutionary stages as the population of composition Z at age 12×10^9 years.

The distribution of stars in the H-R diagram is first found at time t_m for each region, using standard input data. The positions of the stars are then corrected for the structural effect, and the colors are further corrected for blanketing; the resulting integrated color is given in line 7. If all the stars had been formed at time t_f, line 7 would give the properly corrected color at age 12×10^9 years. This would be the case, for example, in model S, where all stars are formed in a single initial burst. However, the presence of younger stars in all models except S means that the lifetime effect has been exaggerated in these models. Line 8 gives the color obtained by applying just the structural and blanketing corrections to the population present at age 12×10^9 years, with standard rates of evolution. An exact treatment of the lifetime effect would give colors somewhere between those of line 7 and line 8. Judging by the dominance of stars born at time t_f relative to those born subsequently, an estimate is made of the lifetime effect by interpolating between these lines, and the final "best guess" is given in line 9. The final correction, the difference between the best estimate of the corrected color and original color, is given in line 10.

For several reasons, the correction does not vary monotonically with $\langle Z_* \rangle$. First, the structural and blanketing effects, especially the latter, are greater for a given $\Delta \log Z$ when late stars dominate; for example, they are smaller in the center of model I than in the center of model D (compare the differences between lines 8 and 3 for these two regions), although the Z values are similar. Second, the importance of the "full" lifetime correction, as used in line 7, depends on the rate of evolution of $B - V$ in the region; for example, this is also smaller in the center of model I than in the center of model D (compare the differences between lines 7 and 8), since the former region evolves more slowly in color so the populations at times t and t_m are less different. Finally, the extent to which the lifetime effect is included in choosing the best estimate between lines 7 and 8 depends on how sharply star formation is peaked at time t_f. In model D, line 7 should provide good estimates of the corrected colors in all regions. In the inner regions of model I, younger stars are nearly as important as those formed at t_f, so there is little lifetime effect.

The corrections derived here should be regarded as only provisional, owing to the obvious, but at present unavoidable, shortcomings of the method. When further systematic calculations are available for the effects of abundance changes on all stages of evolution of Population I stars, and when a wider range of blanketing data is available, covering both longer and shorter wavelengths and more stellar types, it will be necessary and important to revise and extend the present color corrections.

REFERENCES

Aizenman, M. L., Demarque, P., and Miller, R. H. 1969, *Ap. J.*, **155**, 973.
Audouze, J., and Tinsley, B. M. 1974, *Ap. J.*, in press.
Bell, R. A. 1971, *M.N.R.A.S.*, **154**, 343.
Branch, D., and Alexander, J. B. 1973, *M.N.R.A.S.*, **161**, 409.
Cannon, R. D. 1970, *M.N.R.A.S.*, **150**, 111.
Code, A. D., Welch, G. A., and Page, T. L. 1972, in *The Scientific Results from the Orbiting Astronomical Observatory (OAO-2)*, ed. A. D. Code (Washington, D.C.: NASA SP-310), p. 559.
Copeland, H., Jensen, J. O., and Jørgensen, H. E. 1970, *Astr. and Ap.*, **5**, 12.
de Vaucouleurs, G. 1961, *Ap. J. Suppl.*, **5**, 233.
de Vaucouleurs, G., and de Vaucouleurs, A. 1972, *Mem. R.A.S.*, **77**, 1.
Doherty, L. R. 1972, *Ap. J.*, **178**, 727.
Faber, S. M. 1973, *Ap. J.*, **179**, 731.
Gottlieb, D. M., and Bell, R. A. 1972, *Astr. and Ap.*, **19**, 434.
Gunn, J. E., and Gott, J. R. 1972, *Ap. J.*, **176**, 1.
Gunn, J. E., and Ostriker, J. P. 1970, *Ap. J.*, **160**, 979.
Hearnshaw, J. B. 1972, *Mem. R.A.S.*, **77**, 55.
Hodge, P. W. 1973, *Ap. J.*, **182**, 671.
Janes, K. A. 1972, Ph.D. thesis, Yale University.
King, I. R., and Minkowski, R. 1972, in *External Galaxies and Quasi-stellar Objects (I.A.U. Symposium No. 44)*, ed. D. S. Evans (Dordrecht: Reidel), p. 87.
Larson, R. B. 1972, *Nature*, **236**, 21.
———. 1973, *M.N.R.A.S.*, **161**, 133.
———. 1974, *ibid.*, **166**, 585 (Paper I).
Mathews, W. G., and Baker, J. C. 1971, *Ap. J.*, **170**, 241.
McClure, R. D. 1969, *A.J.*, **74**, 50.
Miller, R. H., and Prendergast, K. H. 1962, *Ap. J.*, **136**, 713.
Morton, D. C., and Chevalier, R. A. 1973, *Ap. J.*, **179**, 55.
Nordsiek, K. H. 1973, *Ap. J.*, **184**, 735.
Oemler, A. 1973, Ph.D. thesis, California Institute of Technology.
Oke, J. B. 1971, *Ap. J.*, **170**, 193.
Oke, J. B., and Sandage, A. R. 1968, *Ap. J.*, **154**, 21.
Quirk, W. J., and Tinsley, B. M. 1973, *Ap. J.*, **179**, 69.
Rood, H. J., Page, T., Kintner, E., and King, I. R. 1972, *Ap. J.*, **175**, 627.
Rose, W. K., and Tinsley, B. M. 1974, *Ap. J.*, in press.
Sandage, A. R. 1961, *Ap. J.*, **134**, 916.
———. 1972, *ibid.*, **173**, 485.
———. 1973, *ibid.*, **183**, 711.
Sandage, A. R., and Eggen, O. J. 1969, *Ap. J.*, **158**, 685.
Sargent, W. L. W., Searle, L., and Kowal, C. T. 1974, in *Supernovae and Supernova Remnants*, ed. C. B. Cosmovici (Dordrecht: Reidel), in press.
Sargent, W. L. W., and Tinsley, B. M. 1974, *M.N.R.A.S.*, in press.
Schild, R. E. 1972, *Ap. J.*, **178**, 617.
Searle, L. 1971, *Ap. J.*, **168**, 327.
Searle, L., Sargent, W. L. W., and Bagnuolo, W. G. 1973, *Ap. J.*, **179**, 427.
Spinrad, H., and Taylor, B. J. 1969, *Ap. J.*, **157**, 1279.
———. 1971, *Ap. J. Suppl.*, **22**, 445.
Spinrad, H., Gunn, J. E., Taylor, B. J., McClure, R. D., and Young, J. W. 1971, *Ap. J.*, **164**, 11.
Spinrad, H., Smith, H. E., and Taylor, D. J. 1972, *Ap. J.*, **175**, 649.
Tammann, G. A. 1974, in *Supernovae and Supernova Remnants*, ed. C. B. Cosmovici (Dordrecht: Reidel), in press.
Tifft, W. G. 1969, *A.J.*, **74**, 354.
Tinsley, B. M. 1972*a*, *Astr. and Ap.*, **20**, 383.
———. 1972*b*, *Ap. J. (Letters)*, **173**, L93.
———. 1972*c*, *Ap. J.*, **178**, 319.
———. 1972*d*, *Ap. J. (Letters)*, **178**, L39.
———. 1973, *ibid.*, **184**, L41.

Torres-Peimbert, S. 1971, *Bol. Obs. Tonantzintla y Tacubaya*, **6**, 113.
Trimble, V., and Greenstein, J. L. 1972, *Ap. J.*, **177**, 441.
Van Citters, G. W., and Morton, D. C. 1970, *Ap. J.*, **161**, 695.
van den Bergh, S. 1972, *J.R.A.S. Canada*, **66**, 237.
Weistrop, D. 1972, *A.J.*, **77**, 849.
Welch, G. A., and Forrester, W. T. 1972, *A.J.*, **77**, 333.
Wielen, R. 1974, *Zs. f. Ap.*, **59**, 129.
Woolf, N. 1974, in *Late Stages of Stellar Evolution* (*IAU Symposium No. 66*), ed. R. J. Taylor (Dordrecht: Reidel), in press.
Yahil, A., and Ostriker, J. P. 1973, *Ap. J.*, **185**, 787.

RICHARD B. LARSON
Yale University Observatory, Box 2023 Yale Station, New Haven, CT 06520

BEATRICE M. TINSLEY
The University of Texas at Dallas, Box 30365, Dallas, TX 75230